Massively parallel measurements of molecular interaction kinetics on a microfluidic platform

Marcel Geertz[a], David Shore[a], and Sebastian J. Maerkl[b,1]

[a]Department of Molecular Biology and NCCR program "Frontiers in Genetics," University of Geneva, 30 quai Ernest-Ansermet, CH-1211 Geneva 4, Switzerland; and [b]Institute of Bioengineering, School of Engineering, Ecole Polytechnique Federale de Lausanne, Station 17, CH-1015 Lausanne, Switzerland

Edited by* Curtis G. Callan, Jr., Princeton University, Princeton, NJ, and approved September 5, 2012 (received for review April 11, 2012)

Quantitative biology requires quantitative data. No high-throughput technologies exist capable of obtaining several hundred independent kinetic binding measurements in a single experiment. We present an integrated microfluidic device (k-MITOMI) for the simultaneous kinetic characterization of 768 biomolecular interactions. We applied k-MITOMI to the kinetic analysis of transcription factor (TF)—DNA interactions, measuring the detailed kinetic landscapes of the mouse TF Zif268, and the yeast TFs Tye7p, Yox1p, and Tbf1p. We demonstrated the integrated nature of k-MITOMI by expressing, purifying, and characterizing 27 additional yeast transcription factors in parallel on a single device. Overall, we obtained 2,388 association and dissociation curves of 223 unique molecular interactions with equilibrium dissociation constants ranging from 2×10^{-6} M to 2×10^{-9} M, and dissociation rate constants of approximately 6 s^{-1} to 8.5×10^{-3} s^{-1}. Association rate constants were uniform across 3 TF families, ranging from 3.7×10^{6} M^{-1} s^{-1} to 9.6×10^{7} M^{-1} s^{-1}, and are well below the diffusion limit. We expect that k-MITOMI will contribute to our quantitative understanding of biological systems and accelerate the development and characterization of engineered systems.

biochemistry | biophysics | systems biology

Systems and synthetic biology, as well as the computational models and engineering-based approaches they employ, rely heavily on quantitative data (1, 2). Thus far, efforts in systems biology have mainly focused on cataloging and mapping genomes and proteomes. Genome sequencing and gene expression analysis have provided insight into genome architecture (3–6), and functional genomics approaches, including high-throughput protein-based methods (7–15), mapped network topologies.

Although the number of known protein–protein and protein–DNA interactions is already substantial, the information describing such networks is predominantly qualitative and binary in nature. It is also becoming clear that network topologies alone are not sufficient to model complex biological processes. Precise quantitative information describing every interaction in a network would be tremendously valuable (2), yet binding affinities are known for only a small fraction of interactions (16, 17) and kinetic information hardly exists at all. This dearth of quantitative interaction data is due to a lack of high-throughput technologies capable of measuring kinetic rates of biomolecular interactions. Current methods used for kinetic rate measurements are generally based on surface plasmon resonance (SPR) (18) such as BioRad's ProteOn XPR36 6×6 array system, which measures 36 interactions in a single run. SPR-based measurements have been integrated with microfluidic devices (19, 20) to achieve higher degrees of parallelization (21). Yet proof of concept demonstrations have made use of only a small fraction of the proposed throughput and often restrict their measurements to protein-antibody interactions with high affinities and long half-lives (21–23). On the other hand, low affinity or transient interactions, which are more relevant to biological systems, have not been measured in a high-throughput format. More recent alternatives to SPR, such as nanowire arrays (24), mechanical (25), or optical (26) resonators, are promising methods for generating quantitative kinetic data, but the throughput of these platforms remains severely limited.

Here we present an integrated microfluidic device (19) based on mechanically induced trapping of molecular interactions (MITOMI) (17), capable of characterizing 768 independent biomolecular association and dissociation reactions in parallel (Fig. 1). MITOMI is a versatile platform capable of measuring a broad range of biomolecular interactions, including protein-protein (27), protein-DNA (17, 28), protein-RNA (29), and protein-small molecule (29). The integrated nature of the approach allows for the large-scale on-chip synthesis, purification, and characterization of proteins (30, 31). A recent study by Bates and Quake showed that MITOMI could be adapted to enable the measurement of binding kinetics of a single antibody-antigen interaction (22). However, it has not yet been demonstrated that several hundred independent biomolecular association and dissociation rates could be characterized in parallel on a single integrated platform.

We applied our k-MITOMI platform to the characterization of transcription factor (TF)-DNA interaction kinetics (32). TFs bind to DNA sequences with a wide range of affinities, covering pico- to micromolar dissociation constants (K_d) (17, 33). TF-DNA interactions thus cover the entire range of physiologically relevant affinities (34). Furthermore, TF-DNA interactions are thought to be governed by high (near diffusion limited) association rates and dissociation rate constants with half-lives in the range of seconds to minutes, compared to antibody-antigen half-lives of several hours (35, 36), making TF-DNA interactions technically challenging kinetic reactions to measure. Use of the MITOMI button for "freezing" interactions enables the parallel measurement of many reactions. This approach to "freezing" interactions decouples the number of reactions being investigated from the sampling frequency of the readout method used, and thus is, in this regard, readily scalable.

TF-DNA interactions are biologically relevant as they define transcriptional regulatory networks, which play important roles in essentially all cellular processes. The topologies of these networks have been mapped with a variety of in vivo and in vitro methods, including ChIP-chip (7), ChIP-seq (5), Y1H (37), PBMs (38), SELEX (39, 40), and MITOMI (17, 28). The principal goals of these methods are to establish the genomic binding locations of TFs and to determine their consensus binding sequences, position weight matrixes, and binding energy landscapes (32, 41). Absolute affinities can be acquired with only a few high-throughput methods (17, 42–44), and kinetic information on protein-DNA

Author contributions: M.G., D.S., and S.J.M. designed research; M.G. performed research; M.G. contributed new reagents/analytic tools; M.G. and S.J.M. analyzed data; and M.G., D.S., and S.J.M. wrote the paper.

The authors declare no conflict of interest.

*This Direct Submission article had a prearranged editor.

Freely available online through the PNAS open access option.

[1]To whom correspondence should be addressed. E-mail: sebastian.maerkl@epfl.ch.

This article contains supporting information online at www.pnas.org/lookup/suppl/doi:10.1073/pnas.1206011109/-/DCSupplemental.

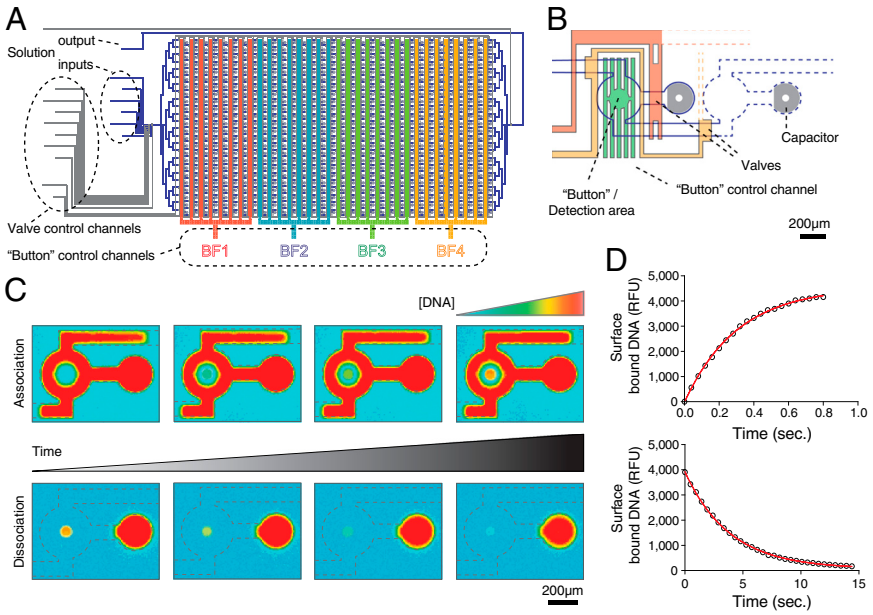

Fig. 1. Schematic overview of the k-MITOMI platform. (*A*) Design drawing of the microfluidic device. Blue and grey lines represent flow and control channels, respectively. The four separately addressable "button" control channels (BF1 to BF4) are highlighted in red, cyan, green, and yellow. (*B*) Schematic of a unit cell. The capacitor is shown in grey. A "neck" valve, shown in red, separates the chamber from the detection area. Individual unit cells are separated from each other by a pair of "sandwich" valves (orange). "Button" membranes (green) are aligned to the center of the detection chamber. (*C*) K-MITOMI process. Controlled opening of the "button" allows for association or dissociation of fluorescently labeled DNA molecules to/from surface immobilized TF. (*D*) Actual association and dissociation traces of DNA molecules to/from the immobilized TF are shown with exponential fits.

interactions has so far only come from low-throughput, complex, and tedious methods such as electrophoretic mobility shift assays (EMSA) (45, 46), SPR (18), isothermal titration calorimetry (ITC) (47), and single molecule experiments (48). Completely defining the kinetic parameters of TF-DNA interactions would provide a better understanding of how TF binding to promoters is integrated and translated into transcriptional output. In fact, the off-rate of TF-DNA interactions may be one of the more important parameters in developing accurate computational models of transcriptional regulation (49, 50).

Using k-MITOMI, we measured the association and dissociation kinetics of the mouse zinc finger Zif268 (Egr1) to its 9 bp long consensus motif, covering all 27 single base substitutions. Zif268 is one of the best studied TFs, and represents the largest TF family (Zn Fingers) (51). We also measured on- and off-rates for the yeast transcription factors Tye7p, Yox1p, and Tbf1p, each against 29 target DNA sequences. To demonstrate the integrated nature of our platform, we expressed, purified, and measured the kinetics of 27 additional yeast TF DBDs, each against 4 DNA sequences in parallel on a single device. In this study we analyzed a total of 684 association and 1,704 dissociation curves from 223 unique molecular interactions (*SI Appendix*, Table S1).

Results

k-MITOMI. To measure kinetic rate parameters, our k-MITOMI platform uses rapid and repeated actuation of the MITOMI buttons to follow the association and dissociation of fluorescently labeled oligonucleotides to a surface-bound TF (Fig. 1). After preparing the surface of the device and localizing protein under the MITOMI detection area, a measurement begins with the buttons in the closed state, protecting the surface-bound protein. Fluorescently labeled oligonucleotides are then allowed to diffuse into the detection area from an adjacent microfluidic chamber. Upon equilibration of the unit cell, the button is opened for a brief duration, during which molecules may interact and associate or dissociate to and from the surface-bound proteins. Button closure terminates each pulse, and in effect "freezes" all 768 reactions. We thus define "pulse duration" as the amount of time that the button is in the open state during which association and dissociation can take place. The entire device is then imaged to determine the quantity of DNA molecules bound to the surface immobilized protein in each of the 768 unit cells. This process is repeated multiple times to give an association curve (Fig. 1 *C* and *D*). Likewise, with molecules bound to the surface-immobilized proteins, dissociation curves can be generated using the same process (Fig. 1 *C* and *D*).

Device Design and Characterization. Our k-MITOMI device consists of 768 unit cells and 3,081 micromechanical elements. Device programming, surface derivatization, and detection steps are performed essentially as previously described (17, 52). We incorporated a number of improvements into the standard MITOMI design. The two main novel design features are a control channel layout that allows for maximal flow rates supplying each button, and fluidic capacitors that buffer pressure build-up from button closure. Button actuation is now performed by gas-filled control channels and computer controlled to ascertain reproducible pulse durations. These changes maximized button actuation speeds and thus optimized the MITOMI platform for kinetic rate measurements.

Button actuation speed determines the temporal resolution of our measurements, which in turn defines the maximum association and dissociation rates that can be accurately measured. To characterize our button actuation speed, we recorded movies of button rise and fall times at 2,000 frames per second (fps) (Fig. 2*A*). The buttons required 10.8 ± 1.0 ms to rise and 7.2 ± 0.4 ms to fall (*SI Appendix*, Fig. S1). This response was uniform across the entire chip in both the lateral and longitudinal directions (*SI Appendix*, Fig. S1). Linear regressions of pulse input signal versus measured pulse duration [the time the button is detached from the surface (Fig. 2*A*)] returned a slope of 1.00 and an x-intercept of 5.00 ± 0.15 ms (Fig. 2*B*). Applying pulse input signals of 50 ms, 100 ms, and 200 ms produced uniform pulse durations of 45.5 ± 0.4 ms, 96.2 ± 0.4 ms, and 196.4 ± 0.5 ms across the entire device (Fig. 2*C*). The button thus responds rapidly and uniformly over a single device as well as across devices

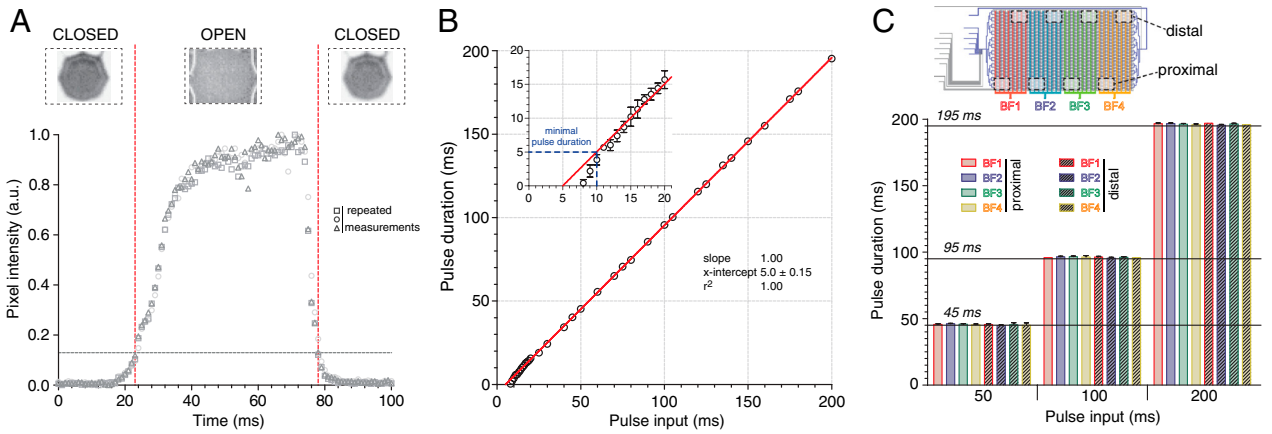

Fig. 2. Characterization of "button" actuation. (*A*) Response profiles of button actuation with a 60 ms pulse input. Movies of button actuation were recorded at 2,000 fps. (*B*) Pulse input signal versus measured pulse duration. A dashed blue line highlights the minimal pulse duration (see *Inset*). (*C*) Pulse durations measured across the entire device respond reliably and uniformly. Solid, horizontal lines indicate the expected pulse durations of 45, 95, and 195 ms.

(Fig. 2 and *SI Appendix*, Fig. S2). Our minimal pulse duration is approximately 5 ms; pulse duration can be controlled with millisecond precision (Fig. 2*B*). A temporal resolution of 10 ms theoretically allows us to measure dissociation rate constants on the order of 10 s^{-1}, assuming a minimum of 10 data points are obtained before depletion occurs.

Kinetic Measurements of Transcription Factor–DNA Interactions. We evaluated our platform by measuring the binding kinetics of the well-characterized mouse C2H2 zinc finger TF Zif268 (48, 53, 54). K-MITOMI devices were aligned to arrays of fluorescently labeled target DNA sequences covering the known consensus sequence of Zif268 and all 27 single-base substitutions. Each sequence was spotted at three different concentrations. A wheat germ lysate spiked with a linear template coding for a His-tagged Zif268 DNA binding domain (Zif268-DBD) was loaded on-chip and incubated for 2 h. In these 2 h Zif268-DBD was expressed, surface immobilized via an anti-His antibody, and finally purified by exchanging the wheat germ lysate with PBS buffer. Kinetic association and dissociation curves were measured as described above (Fig. 1).

We measured the dissociation rates of the 28 target DNA sequences at 11 different pulse durations ranging from 200 ms to 10 s (Fig. 3 *A* and *B*, *SI Appendix*, Fig. S3 and Table S3). In total, we collected 924 dissociation curves consisting of 18,228 data points. We found that the measured dissociation rates systematically varied as a function of the pulse duration, indicating that repeated button opening or closing lead to an increased loss of bound material. Likely sources of this additional loss of bound molecules could be due to dissociation of molecules while the "button" membrane is depressed (17), or during the process of button opening due to hydrodynamic shear forces. Because we gathered dissociation data over a large range of pulse durations and target DNA sequences, we were able to determine that the observed dissociation rates are linearly dependent on the pulse duration (*SI Appendix*, Fig. S4). To calculate dissociation rate constants at infinite pulse duration, we extrapolated our data by linear regression and retrieved k_{off} values from the y-intercepts in a "k_{off}" vs. "1/pulse duration" plot (Fig. 3 *A* and *B* and *SI Appendix*, Fig. S4). We found that the slopes of the linear regressions were not sequence dependent, whereas the extrapolated y-intercepts scaled with target DNA affinity (Fig. 3*B*). Fitting a global slope gave an average goodness of fit of $r^2 = 0.87$ (*SI Appendix*, Fig. S4). To determine whether our extrapolated k_{off} values are equivalent to actual off-rates, we measured the dissociation of surface-bound DNA in real-time without the use of the button, synonymous with an infinite pulse duration (*SI Appendix*, Fig. S5). Real-time and k-MITOMI measurements are in good agreement with $1.31 \pm 0.1 \times 10^{-2}$ s^{-1} compared to $1.64 \pm 0.6 \times 10^{-2}$ s^{-1} for the consensus sequence, and $4.94 \pm 0.5 \times 10^{-2}$ s^{-1} compared to $5.21 \pm 0.8 \times 10^{-2}$ s^{-1} for a sequence variant at zinc finger 3 (F3-GTG; instead of GCG), respectively (*SI Appendix*, Fig. S5). For the 28 target DNA sequences that cover a range of 2.62×10^{-9} M to 1.82×10^{-6} M K_d, we observed a corresponding range of dissociation rates of 1.64×10^{-2} s^{-1} to 4.98 s^{-1} (Fig. 3 *A* and *B*).

Association rate measurements are more challenging to measure as they also depend on the concentration of target sequence present in each chamber. We therefore measured the association of all 28 target sequences over 3 different concentrations, each at 4 pulse durations, generating a total of 336 association curves and 4,032 data points (Fig. 3 *C* and *D* and *SI Appendix*, Fig. S6). The pulse duration had only a negligible effect on the measured association rate constants (Fig. 3*D*). Unlike for the dissociation rates, we observed that the association rate constants varied considerably less as a function of K_d, ranging from 2.74×10^6 M^{-1} s^{-1} to 7.01×10^6 M^{-1} s^{-1}. We calculated K_d values from our dissociation and association rate measurements and compared these with independently measured K_d values for each of the 28 sequences on a MITOMI device. Dissociation constants derived from both platforms correlated linearly with a Pearson and Spearmen correlation coefficient of 0.87 and 0.98, respectively (Fig. 3*E*). The association and dissociation rate constants measured on our k-MITOMI device thus agree well with independent MITOMI measurements (Fig. 3*E*), real-time measurements (*SI Appendix*, Fig. S5), and previously published values (*SI Appendix*, Table S2). Sequence logos derived from k-MITOMI k_{off} measurements and calculated K_d values (k_{off}/k_{on}) compare well to sequence logos obtained with PBM, HT-SELEX, and B1H (*SI Appendix*, Fig. S7).

We found that the binding affinity of Zif268 to DNA over a broad sequence space with nM to μM affinity is almost exclusively determined by its dissociation rate (Fig. 3*F* and *SI Appendix*, Table S3). Eighty-nine percent of Zif268's affinity is determined by the dissociation rate, as shown by a positive regression slope of 0.89. Sequence-specific affinity is only marginally determined by the association rate (slope of −0.11; Fig. 3*F*). This confirms theoretical expectations that k_{off} should be the sole determinant of binding specificity (55, 56). We tested the generality of this finding by measuring the binding kinetics of three yeast TFs from different DBD families: Tye7p (bHLH), Yox1p (homeobox), and Tbf1p (SANT). Measured dissociation rates across the DNA sequence spectrum ranged between 8.1×10^{-3} s^{-1} to 2.58×10^{-1} s^{-1}, 5.06×10^{-1} s^{-1} to 1.42 s^{-1}, and 7.65×10^{-1} s^{-1} to 2.58 s^{-1} for Tye7p, Yox1p, and Tbf1p, respectively (Fig. 3*F*). Association rate constants did not vary significantly across these

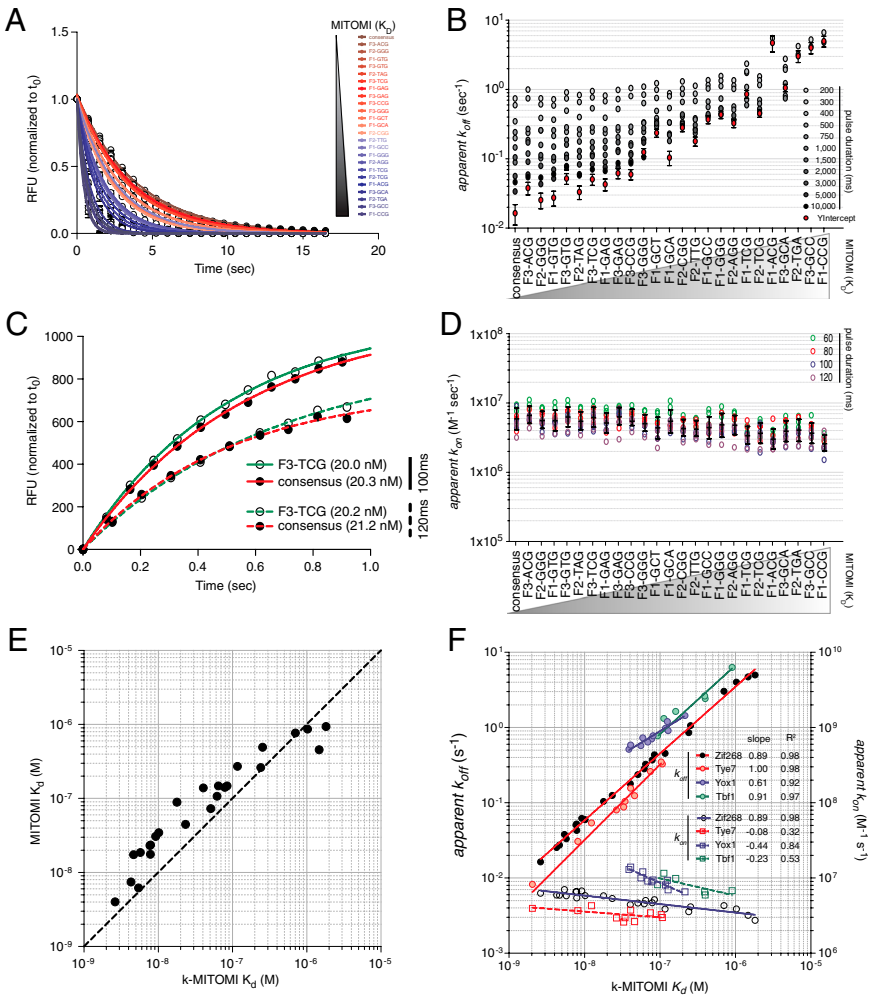

Fig. 3. Comprehensive kinetic measurements of transcription factor-DNA interactions. (*A*) Dissociation of Zif268-DNA complexes measured with a 750 ms pulse duration. Normalized, surface bound DNA traces are shown with exponential fits. Color code shows the separately measured K_d values (red to blue = high to low binding affinity). (*B*) Plot of K_d ranked Zif268 dissociation rate constants derived across different pulse durations, as well as extrapolated rate constants. (*C*) Association of two cognate DNA targets with Zif268 at two different pulse durations and comparable DNA concentration. (*D*) Plot of K_d ranked Zif268 association rate constants derived across different pulse durations. (*E*) Comparison of K_d values calculated from k-MITOMI association and dissociation rate constants to K_d values determined from saturation binding curves measured with MITOMI. (*F*) Zif268, Tye7p, Yox1p, and Tbf1p dissociation and association rate constants plotted against calculated K_d values.

three TFs, with measured values of 2.56×10^6 M^{-1} s^{-1} to 4.22×10^6 M^{-1} s^{-1}, 6.47×10^6 M^{-1} s^{-1} to 1.38×10^7 M^{-1} s^{-1}, and 5.88×10^6 M^{-1} s^{-1} to 1.14×10^7 M^{-1} s^{-1} for Tye7p, Yox1p, and Tbf1p, respectively. In all cases dissociation rates dominate binding specificities as shown by regression slopes of 1.00, 0.61, and 0.91 for Tye7p, Yox1p, and Tbf1p, respectively.

Characterization of a Broad Spectrum of TFs. Each k-MITOMI unit cell can be loaded independently by cospotting linear expression templates and dsDNA molecules, followed by on-chip protein expression, purification, and characterization (30). To demonstrate the integrated nature of our k-MITOMI platform, we loaded our device with linear expression templates coding for 47 TFs across diverse DBD families (57, 58) and cospotted 1 corresponding cognate and 3 noncognate sequences for a total of 188 TF-DNA combinations. Thirty-three TFs (70%) expressed on-chip and bound DNA; we were able to measure dissociation rates for 27 (57%) of these 33 TFs. Eight TFs (17%) expressed on chip but bound DNA only marginally, and 6 TFs (13%) failed to express (Fig. 4*A*).

We monitored the dissociation of bound DNA at pulse durations between 200 and 2,000 ms and observed dissociation rate constants in the range of 8.11×10^{-3} s^{-1} to 6.52×10^{-1} s^{-1} (Fig. 4*B*). The slowest dissociation rates of 8.11×10^{-3} s^{-1} and 1.07×10^{-2} s^{-1} were observed for Tye7p and Cin5p, bHLH, and bZIP TFs, respectively. Zinc-finger TFs such as Met32p showed intermediate to fast dissociation rates ranging from 1.89×10^{-2} s^{-1} to 3.04×10^{-1} s^{-1}, while Gal4 TFs were uniformly fast, with rates of 2.77×10^{-1} s^{-1} or higher. The dissociation rates for the Gal4 family of TFs are fast because we measured the dissociation of a monomer rather than the dimer (59).

Another important parameter in understanding TF-DNA binding specificity is the binding kinetics to noncognate DNA (60). Nonspecific binding energies determine target search times (61). To measure these kinetic rates, we permuted TF-DNA

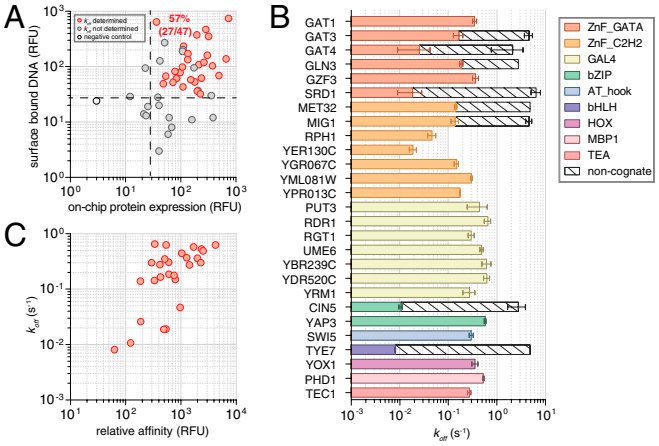

Fig. 4. Integrated kinetic measurements of a broad spectrum of transcription factors. (*A*) Surface bound cognate target DNA values are plotted against TF expression levels. (*B*) Dissociation rate constants of TF-DNA complexes for consensus and noncognate target DNAs. Color code highlights the different DBD families. (*C*) Dissociation rate constants of all TF-consensus DNA dyads are plotted against MITOMI derived relative affinity measurements.

dyads and measured noncognate pairs. In total, we successfully measured 8 such noncognate TF-DNA interactions and obtained dissociation rate constants between 2.09 s^{-1} to 6.49 s^{-1} (Fig. 4*B*). We also observed DNA binding for the remaining noncognate TF-DNA interactions, but the dissociation rates of these interactions exceeded our temporal resolution obtained with a 200 ms pulse duration. The difference in cognate and noncognate dissociation rates, and by extension affinity, of these 8 TFs is at least 1 order of magnitude (Gln3p), and can be as high as approximately 3 orders of magnitude (Tye7p). This indicates that a functional TF requires an affinity difference between its consensus site and nonspecific background of at least one order of magnitude or higher, with a minimal dissociation rate from nonspecific DNA of at least 2 s^{-1}. Finally, plotting k_{off} values against independently derived relative K_d values confirmed the dominance of dissociation rate constants in establishing affinity across different TF families (Fig. 4*C*) as observed for Zif268, Tye7p, Yox1p, and Tbf1p (Fig. 3*F*).

Discussion

We developed an integrated and versatile microfluidic platform for the high-throughout kinetic characterization of biomolecular interactions. Our k-MITOMI platform measures 768 unique kinetic interactions in parallel on a single device. In this report, we collected a total of 684 association and 1,704 dissociation curves for 223 unique molecular interactions. We measured molecular interactions covering an affinity range of 3 orders of magnitude (2×10^{-6} M to 2×10^{-9} M) and an equally broad range of dissociation rates (approximately 6 s^{-1} to 8.5×10^{-3} s^{-1}). Based on the study of Bates and Quake and rates measured in this study, k-MITOMI can capture association rates in the range of 4.4×10^4 M^{-1} s^{-1} to 1.39×10^7 M^{-1} s^{-1} (22). Our platform drastically increases the throughput for kinetic rate measurements by parallelizing the process, but also simplifies and streamlines the entire experimental approach by integrating protein expression, purification, and characterization on a single platform.

We applied our k-MITOMI platform to a relevant system by characterizing the binding kinetics of a large number of TF-DNA interactions. We validated our platform by comprehensively measuring the binding kinetics of the well-characterized transcription factor Zif268 and the transcription factors Tye7p, Yox1p, and Tbf1p. We demonstrated the integrated nature of our platform by characterizing an additional 27 TFs in parallel. These measurements provide a broad overview of the kinetics governing TF-DNA interactions.

It should be noted that the equilibrium dissociation constants and kinetic rates for Zif268 binding to its consensus sequence have been measured using a number of approaches, but the reported on- and off-rates vary over 5 and 3 orders of magnitude, respectively (*SI Appendix*, Table S2). It is thus difficult to determine generally established values for these constants, as measurements strongly depend on the techniques and reaction conditions used. Nonetheless, our kinetic measurements agree with thermodynamic measurements (Fig. 3*E*) and more importantly the measured kinetic rates return the same binding specificity of Zif268 as determined by other methods, including PBMs, HT-SELEX, and B1H (*SI Appendix*, Fig. S7), providing a measure of confidence that the rates determined by k-MITOMI reflect the biophysics of Zif268. Furthermore, the 10- to 100-fold differences between consensus sequence and noncognate sequences determined here are in agreement with order of magnitude differences in binding modes determined in vivo (62).

We experimentally validated that the affinity of these transcription factors for DNA is determined predominantly by the dissociation rate. Surprisingly, the affinity of TFs from different families also seems to be mainly determined by the dissociation rate, while the observed association rates varied only slightly across families. Kinetic rates can thus be obtained for TF-DNA interactions on a k-MITOMI device with relative ease, requiring only off-rate measurements. Measurements of affinity constants and association rates generally require multiple measurements at different ligand concentrations, whereas off-rate measurements are concentration independent. This is significant, as it increases MITOMI throughput by about an order of magnitude and each unit cell returns a full kinetic binding profile. More generally, the fact that association rate constants appear to be uniform and diffusion limited across TF families will make it considerably easier to derive kinetic rates for any TF, as only a thermodynamic measurement or an off-rate measurement is required. Nonetheless, it will also be important to assess the effect of molecular size, solvent viscosity, and ionic strength on association and dissociation rates. Some limitations of the current assay geometry, with TFs immobilized to the surface and solution phase DNA oligos, include the fact that the diffusion coefficient of the TF does not contribute to the observed association rate. Possible surface effects arising from our short DNA oligos binding bivalently to two TFs may also skew the observed off-rates, giving rise to slightly slower dissociation rates, than would be otherwise observed. However, steric considerations of the surface chemistry, the length of oligos used, and their sequence all make it unlikely that bivalent binding is occurring. These issues could be resolved by inverting the current assay geometry by immobilizing the DNA targets on the surface and observing the association and dissociation of labeled TFs.

We determined the dissociation rate of 8 TFs to nonspecific DNA and determined that the slowest dissociation rate was approximately 2 s^{-1} and that the smallest difference between nonspecific and specific binding was at least one order of magnitude. A minimum dissociation rate of 2 s^{-1} may be required to allow search times to remain low by avoiding being trapped for considerable lengths of time on nonspecific DNA (61). A slower dissociation rate is necessary for the consensus site to increase TF dwell-time at the target location. These parameters can be considered guidelines for engineering novel transcription factors (63, 64). Our data may also help guide and implement computational models of transcriptional regulation.

MITOMI has been shown to be a versatile platform for characterizing a plethora of molecular interactions. The prototype k-MITOMI platform presented here significantly extends the informational content of MITOMI measurements by measuring association and dissociation rates of 768 interactions on a single device. Our k-MITOMI platform will aid systems biology in the quantitative characterization of biological networks. Synthetic biology also heavily relies on our ability to rapidly generate and quantitatively characterize engineered components and systems. New technologies such as k-MITOMI will be critically important in developing a quantitative understanding of biological systems and in our ability to engineer them.

Methods

The k-MITOMI devices were fabricated as previously described (19). Linear templates for cell-free expression of transcription factors were also generated as previously described (17), and all primer sequences are provided in *SI Appendix*, Table S4. Fluorescently labeled dsDNA targets were generated by a Klenow extension reaction (17), and the target sequences are given in *SI Appendix*, Table S3. DNA targets and linear expression templates were arrayed onto epoxy coated glass substrates using a QArray2 DNA microarrayer (GenetiX). Printed glass substrates were aligned to a microfluidic device and bonded overnight at 40 °C. Generation of surface chemistry was performed as previously described (17). Proteins were expressed either on-chip or in bulk reactions using a wheat germ-based ITT kit (TNT T7 Quick Coupled Transcription/Translation System, Promega) supplemented with FluoroTect $Green_{Lys}$ BODIPY-FL charged lysine tRNA (Promega). All microfluidic control lines were regulated by manual three-way valves, except for the button control line, which was actuated by a solenoid valve controlled by a LabView (National Instruments) program for accurate timing. Association and dissociation of fluorescently labeled dsDNA targets to surface immobilized transcription factors were imaged with an ArrayWorX (Applied Precision) microarray

scanner. Each device scan, representing a single time-point, was subsequently quantitated using GenePix software (Molecular Devices). More detailed descriptions of methods and materials can be found in the *SI Appendix*.

ACKNOWLEDGMENTS. We thank Felix Naef, Thanos D. Halazonetis, and Leonid Mirny for valuable discussions. This work was supported by SystemsX.ch DynamiX-RTD Grant 2008/005.

1. Arkin A (2008) Setting the standard in synthetic biology. *Nat Biotechnol* 26:771–774.
2. Kitano H (2002) Systems biology: A brief overview. *Science* 295:1662–1664.
3. Kasowski M, et al. (2010) Variation in transcription factor binding among humans. *Science* 328:232–235.
4. Nagalakshmi U, et al. (2008) The transcriptional landscape of the yeast genome defined by RNA sequencing. *Science* 320:1344–1349.
5. Johnson DS, Mortazavi A, Myers RM, Wold B (2007) Genome-wide mapping of in vivo protein-DNA interactions. *Science* 316:1497–1502.
6. Hawkins RD, Hon GC, Ren B (2010) Next-generation genomics: An integrative approach. *Nat Rev Genet* 11:476–486.
7. Harbison CT, et al. (2004) Transcriptional regulatory code of a eukaryotic genome. *Nature* 431:99–104.
8. Walhout AJ, et al. (2000) Protein interaction mapping in *C. elegans* using proteins involved in vulval development. *Science* 287:116–122.
9. Schuldiner M, et al. (2005) Exploration of the function and organization of the yeast early secretory pathway through an epistatic miniarray profile. *Cell* 123:507–519.
10. Collins SR, et al. (2007) Functional dissection of protein complexes involved in yeast chromosome biology using a genetic interaction map. *Nature* 446:806–810.
11. Hutchins JRA, et al. (2010) Systematic analysis of human protein complexes identifies chromosome segregation proteins. *Science* 328:593–599.
12. Newman JRS, Keating AE (2003) Comprehensive identification of human bZIP interactions with coiled-coil arrays. *Science* 300:2097–2101.
13. Lieb JD, Liu X, Botstein D, Brown PO (2001) Promoter-specific binding of Rap1 revealed by genome-wide maps of protein-DNA association. *Nat Genet* 28:327–334.
14. Gavin A-C, et al. (2002) Functional organization of the yeast proteome by systematic analysis of protein complexes. *Nature* 415:141–147.
15. Uetz P, et al. (2000) A comprehensive analysis of protein-protein interactions in Saccharomyces cerevisiae. *Nature* 403:623–627.
16. Jones RB, Gordus A, Krall JA, MacBeath G (2006) A quantitative protein interaction network for the ErbB receptors using protein microarrays. *Nature* 439:168–174.
17. Maerkl SJ, Quake SR (2007) A systems approach to measuring the binding energy landscapes of transcription factors. *Science* 315:233–237.
18. Fägerstam LG, Frostell-Karlsson A, Karlsson R, Persson B, Rönnberg I (1992) Biospecific interaction analysis using surface plasmon resonance detection applied to kinetic, binding site and concentration analysis. *J Chromatogr* 597:397–410.
19. Thorsen T, Maerkl SJ, Quake SR (2002) Microfluidic large-scale integration. *Science* 298:580–584.
20. Gervais T, Jensen KF (2006) Mass transport and surface reactions in microfluidic systems. *Chem Eng Sci* 61:1102–1121.
21. Ouellet E, et al. (2010) Parallel microfluidic surface plasmon resonance imaging arrays. *Lab Chip* 10:581–588.
22. Bates SR, Quake SR (2009) Highly parallel measurements of interaction kinetic constants with a microfabricated optomechanical device. *Appl Phys Lett* 95:73705.
23. Singhal A, Haynes CA, Hansen CL (2010) Microfluidic measurement of antibody-antigen binding kinetics from low-abundance samples and single cells. *Anal Chem* 82:8671–8679.
24. Zheng G, Patolsky F, Cui Y, Wang WU, Lieber CM (2005) Multiplexed electrical detection of cancer markers with nanowire sensor arrays. *Nat Biotechnol* 23:1294–1301.
25. Kwon TY, et al. (2007) In situ real-time monitoring of biomolecular interactions based on resonating microcantilevers immersed in a viscous fluid. *Appl Phys Lett* 90:223903.
26. Mandal S, Goddard JM, Erickson D (2009) A multiplexed optofluidic biomolecular sensor for low mass detection. *Lab Chip* 9:2924–2932.
27. Gerber D, Maerkl SJ, Quake SR (2009) An in vitro microfluidic approach to generating protein-interaction networks. *Nat Methods* 6:71–74.
28. Fordyce PM, et al. (2010) De novo identification and biophysical characterization of transcription-factor binding sites with microfluidic affinity analysis. *Nat Biotechnol* 28:970–975.
29. Einav S, et al. (2008) Discovery of a hepatitis C target and its pharmacological inhibitors by microfluidic affinity analysis. *Nat Biotechnol* 26:1019–1027.
30. Maerkl SJ, Quake SR (2009) Experimental determination of the evolvability of a transcription factor. *Proc Natl Acad Sci USA* 106:18650–18655.
31. Maerkl SJ (2011) Next generation microfluidic platforms for high-throughput protein biochemistry. *Curr Opin Biotechnol* 22:59–65.
32. Geertz M, Maerkl SJ (2010) Experimental strategies for studying transcription factor-DNA binding specificities. *Brief Funct Genomics* 9:362–373.
33. Greisman HA, Pabo CO (1997) A general strategy for selecting high-affinity zinc finger proteins for diverse DNA target sites. *Science* 275:657–661.
34. Tanay A (2006) Extensive low-affinity transcriptional interactions in the yeast genome. *Genome Res* 16:962–972.
35. Nelson HC, Sauer RT (1985) Lambda repressor mutations that increase the affinity and specificity of operator binding. *Cell* 42:549–558.
36. Malmborg AC, Borrebaeck CA (1995) BIAcore as a tool in antibody engineering. *J Immunol Methods* 183:7–13.
37. Deplancke B, et al. (2006) A gene-centered *C. elegans* protein-DNA interaction network. *Cell* 125:1193–1205.
38. Badis G, et al. (2009) Diversity and complexity in DNA recognition by transcription factors. *Science* 324:1720–1723.
39. Jolma A, et al. (2010) Multiplexed massively parallel SELEX for characterization of human transcription factor binding specificities. *Genome Res* 20:861–873.
40. Zhao Y, Granas D, Stormo GD (2009) Inferring binding energies from selected binding sites. *PLoS Comput Biol* 5:e1000590.
41. Stormo GD, Zhao Y (2010) Determining the specificity of protein–DNA interactions. *Nat Rev Genet* 11:751–760.
42. Kinney JB, Murugan A, Callan CGJ, Cox EC (2010) Using deep sequencing to characterize the biophysical mechanism of a transcriptional regulatory sequence. *Proc Natl Acad Sci USA* 107:9158–9163.
43. Nutiu R, et al. (2011) Direct measurement of DNA affinity landscapes on a high-throughput sequencing instrument. *Nat Biotechnol* 29:659–664.
44. Siggers T, Duyzend MH, Reddy J, Khan S, Bulyk ML (2011) Non-DNA-binding cofactors enhance DNA-binding specificity of a transcriptional regulatory complex. *Mol Syst Biol* 7:555.
45. Garner MM, Revzin A (1981) A gel electrophoresis method for quantifying the binding of proteins to specific DNA regions: Application to components of the Escherichia coli lactose operon regulatory system. *Nucleic Acids Res* 9:3047–3060.
46. Fried M, Crothers DM (1981) Equilibria and kinetics of lac repressor–operator interactions by polyacrylamide gel electrophoresis. *Nucleic Acids Res* 9:6505–6525.
47. Oda M, Furukawa K, Ogata K, Sarai A, Nakamura H (1998) Thermodynamics of specific and non-specific DNA binding by the c-Myb DNA-binding domain. *J Mol Biol* 276:571–590.
48. Nalefski EA, Nebelitsky E, Lloyd JA, Gullans SR (2006) Single-molecule detection of transcription factor binding to DNA in real time: Specificity, equilibrium, and kinetic parameters. *Biochemistry* 45:13794–13806.
49. Mirny L, Slutsky M, Wunderlich Z, Tafvizi A (2009) How a protein searches for its site on DNA: The mechanism of facilitated diffusion. *J Phys A Math Theor* 42:434013.
50. Wunderlich Z, Mirny LA (2008) Spatial effects on the speed and reliability of protein-DNA search. *Nucleic Acids Res* 36:3570–3578.
51. Tupler R, Perini G, Green MR (2001) Expressing the human genome. *Nature* 409:832–833.
52. Geertz M, Rockel S, Maerkl SJ (2012) A high-throughput microfluidic method for generating and characterizing transcription factor mutant libraries. *Methods Mol Biol* 813:107–123.
53. Bulyk ML, Huang X, Choo Y, Church GM (2001) Exploring the DNA-binding specificities of zinc fingers with DNA microarrays. *Proc Natl Acad Sci USA* 98:7158–7163.
54. Kim JS, Pabo CO (1998) Getting a handhold on DNA: Design of poly-zinc finger proteins with femtomolar dissociation constants. *Proc Natl Acad Sci USA* 95:2812–2817.
55. Halford S (2009) An end to 40 years of mistakes in DNA-protein association kinetics? *Biochem Soc Trans* 37:343–348.
56. Halford S, Marko J (2004) How do site-specific DNA-binding proteins find their targets? *Nucleic Acids Res* 32:3040–3052.
57. Badis G, et al. (2008) A library of yeast transcription factor motifs reveals a widespread function for Rsc3 in targeting nucleosome exclusion at promoters. *Mol Cell* 32:878–887.
58. Zhu C, et al. (2009) High-resolution DNA binding specificity analysis of yeast transcription factors. *Genome Res* 19:556–566.
59. Hong M, et al. (2008) Structural basis for dimerization in DNA recognition by Gal4. *Structure* 16:1019–1026.
60. Slutsky M, Mirny L (2004) Kinetics of protein-DNA interaction: Facilitated target location in sequence-dependent potential. *Biophys J* 87:4021–4035.
61. Slutsky M, Mirny LA (2004) Kinetics of protein-DNA interaction: Facilitated target location in sequence-dependent potential. *Biophys J* 87:4021–4035.
62. Phair RD, et al. (2004) Global nature of dynamic protein-chromatin interactions in vivo: Three-dimensional genome scanning and dynamic interaction networks of chromatin proteins. *Mol Cell Biol* 24:6393–6402.
63. Urnov FD, Rebar EJ, Holmes MC, Zhang HS, Gregory PD (2010) Genome editing with engineered zinc finger nucleases. *Nat Rev Genet* 11:636–646.
64. Sanjana NE, et al. (2012) A transcription activator-like effector toolbox for genome engineering. *Nat Protoc* 7:171–192.